

Moduli Spaces of Gauge Theories from Dimer Models: Proof of the Correspondence

Sebastián Franco¹ and David Vegh²

¹ *Joseph Henry Laboratories,
Princeton University,
Princeton, NJ 08544, USA. **

² *Center for Theoretical Physics,
Massachusetts Institute of Technology,
Cambridge, MA 02139, USA.†*

sfranco@feynman.princeton.edu, dvegh@mit.edu

ABSTRACT:

Recently, a new way of deriving the moduli space of quiver gauge theories that arise on the world-volume of D3-branes probing singular toric Calabi–Yau cones was conjectured. According to the proposal, the gauge group, matter content and tree-level superpotential of the gauge theory is encoded in a periodic tiling, the dimer graph. The conjecture provides a simple procedure for determining the moduli space of the gauge theory in terms of perfect matchings.

For gauge theories described by periodic quivers that can be embedded on a two-dimensional torus, we prove the equivalence between the determination of the toric moduli space with a gauged linear sigma model and the computation of the Newton polygon of the characteristic polynomial of the dimer model. We show that perfect matchings are in one-to-one correspondence with fields in the linear sigma model. Furthermore, we prove that the position in the toric diagram of every sigma model field is given by the slope of the height function of the corresponding perfect matching.

*Research supported by the National Science Foundation Grant No. PHY- 0243680.

†Research supported in part by the CTP and the LNS of MIT and the U.S. Department of Energy under cooperative agreement #DE-FC02-94ER40818.

Contents

1. Introduction	1
2. Toric quivers and brane tilings	3
2.1 Geometry of the tiling embedding from conformal invariance	7
2.2 Height function	8
3. Toric geometry from gauge theory	9
4. The conjecture	12
5. The proof	13
5.1 Solving F-term conditions: gauge transformations and magnetic coordinates	14
5.2 The GLSM fields are perfect matchings	17
5.3 Height changes as positions in a toric diagram	19
6. Conclusions	22
7. Appendix	23

1. Introduction

According to the AdS/CFT correspondence [1, 2, 3, 4], the large N 't Hooft limit of $\mathcal{N} = 4$ $SU(N)$ super Yang Mills is equivalent to type IIB String Theory on $AdS \times S^5$ with N units of Ramond–Ramond 5-form flux on the S^5 . The $\mathcal{N} = 4$ gauge theory arises as the worldvolume theory of a stack of N D3-branes in flat ten dimensional space. Since its original formulation, the AdS/CFT correspondence has been extended to and checked in a variety of more realistic, less supersymmetric situations. The worldvolume theory of D3-branes over a singular Calabi–Yau threefold is an $\mathcal{N} = 1$ quiver gauge theory [5, 6]. The structure of the gauge theory reflects the properties of the singular manifold. When the Calabi–Yau is a metric cone over an X_5 Sasaki–Einstein manifold, the corresponding dual is type IIB string theory on $AdS_5 \times X_5$.

Toric Calabi–Yau’s are a particularly simple, yet extremely rich, subset in the space of Calabi–Yau threefolds. Their simplicity resides in that they are defined by a relatively small amount of combinatorial data and can be constructed in terms of two-dimensional gauged linear sigma models.

Recently, we have witnessed remarkable progress in our understanding of $\mathcal{N} = 1$ superconformal field theories, their embedding in string theory and their AdS/CFT duals. We now review an abbreviated list of such developments. On the purely field theoretic front, the a-maximization principle [7] has been a major breakthrough, permitting the computation of R-charges for arbitrary $\mathcal{N} = 1$ superconformal theories. In [8, 9], explicit metrics for an infinite family of Sasaki–Einstein 5-manifolds denoted $Y^{p,q}$ were found. The metric cones over these manifolds are toric [10] and the corresponding gauge theories have been determined [11]. Afterwards, a larger set of metrics dubbed $L^{a,b,c}$, containing the $Y^{p,q}$ ’s as particular cases, was discovered [12, 13, 14]. Again, the corresponding cones are toric and the dual gauge theories were identified [15, 16, 17]. With these theories, we passed from having a couple of examples in which the explicit $AdS_5 \times X_5$ metric and the field theory dual were known (X_5 being S^5 , $T^{1,1}$ and their orbifolds) to an infinite number of such pairs. In [18], the geometric dual of a-maximization, Z-minimization, was found. Using Z-minimization it is possible to compute the volume of subcycles in a toric variety using solely the information in the toric diagram. Further developments in the subject appeared in [19, 20, 21].

In parallel, there has been considerable advancement in the techniques for deriving gauge theories on D-branes over singularities. Some of the approaches are partial resolution [22, 23, 24] of orbifold singularities [5, 6], exceptional collections [25, 26, 27, 28, 29, 30, 31, 32] and dimer methods [33, 34, 15, 35, 36, 37], the subject of this paper. For toric manifolds, dimers have proved to be very strong in comparison to alternative approaches, producing the most vast set of results together with an appealing elegance and extreme computational simplicity.

As a result of these developments the paradigm under which we look for and test AdS/CFT pairs, at least in the case of toric singularities, has changed. Dimer methods immediately provide the gauge theory for a given toric geometry. Next, we can perform non-trivial checks comparing R-charges and central charges of the field theory, determined with a-maximization, to the volumes of supersymmetric cycles in the singular geometry, which can be computed without explicit knowledge of the metric thanks to Z-minimization.

The dimer method approach to quiver theories on D-branes over toric singularities was initiated in [33], where a striking correspondence between the perfect matching partition function and the toric diagram of the underlying geometry was observed. The idea was fully developed in [34], where the rules for constructing a tiling on which dimers live for an arbitrary toric quiver were established. A physical interpretation of this tiling as a configuration NS5 and D5-branes was also proposed. In addition, [34] conjectured a specific correspondence between GLSM fields and perfect matchings, noticing also how perfect matchings are natural variables to solve F-term equations. This correspondence, which we call Mathematical Dimer Conjecture in this paper, leads to impressive simplifications in the study of branes on toric singularities and lies at the core of the breakthrough of the dimer ideas. The main result of this paper is the proof of the Mathematical Dimer Conjecture.

Until recently, finding the tiling for a particular theory was somewhat *ad hoc*. A major breakthrough was made in [35], by interpreting R-charges as angles in the tiling. Furthermore, based on the observation that the so called zig-zag paths are in one-to-one correspondence with the edges of the toric diagram, the Fast Inverse Algorithm was established which is by now the most efficient tool for computing the quiver and the superpotential from the toric diagram of a toric non-compact Calabi-Yau. A physical realization of the tilings, which supports the proposal of [34], and a proof of the Fast Inverse Algorithm was recently derived in [36] using mirror symmetry.

In order to provide a self-contained presentation, we devote Sections 2 and 3 to review background material. Section 2 discusses the main concepts in toric quivers, brane tilings and dimer models. Section 3 presents the gauged linear sigma model (GLSM) approach for computing toric moduli spaces of toric gauge theories. In Section 4 we present the conjecture of [34], splitting it into the Mathematical and Physical dimer conjectures. Finally, we prove the Mathematical Dimer Conjecture in Section 5. We illustrate all discussions in the paper with the relatively non-trivial example of a quiver theory for D3-branes probing a complex cone over the second del Pezzo surface.

2. Toric quivers and brane tilings

We consider the $\mathcal{N} = 1$ superconformal gauge theories that live on the worldvolume of a stack of N D3-branes probing a non-compact toric Calabi-Yau 3-fold. For every singularity, the gauge theory on the D3-branes is not unique. In fact, we have an infinite number of gauge theories connected by Seiberg duality [38, 39, 40, 25, 41] that flow to the same universality class in the infrared limit. Every gauge theory is specified by a gauge group and a matter content, which are encoded in a quiver diagram, and a superpotential. We will concentrate on a particular subset of this infinite set of dual theories, denoted **toric phases**. A toric phase is defined as a phase in which the gauge group is $\prod SU(N)$, i.e. the ranks of all gauge group factors are the same. Non-toric phases are obtained by Seiberg duality on a node for which the number of flavors is larger than twice the number of colors. The fact that the probed geometry is an affine toric variety constraints the possible structure of the superpotential. It has to be such that all F-term equations are of the form “*monomial* = *monomial*”. This constraint is dubbed the **toric condition** [42] and can be rephrased by saying that every field in the quiver must appear exactly in two terms of the superpotential, with both terms having opposite signs. In addition, all superpotential coefficients can be normalized to 1 by rescaling the fields.

Figure 1 shows one toric phase for the complex cone over dP_2 [24, 42], usually referred to as Model II. The corresponding superpotential is given by

$$\begin{aligned}
W = & [X_{34}X_{45}X_{53}] - [X_{53}Y_{31}X_{15} + X_{34}X_{42}Y_{23}] \\
& + [Y_{23}X_{31}X_{15}X_{52} + X_{42}X_{23}Y_{31}X_{14}] - [X_{23}X_{31}X_{14}X_{45}X_{52}]
\end{aligned}
\tag{2.1}$$

where we have grouped terms to make a \mathbb{Z}_2 global symmetry that acts by interchanging nodes $1 \leftrightarrow 2$ and $4 \leftrightarrow 5$ and charge conjugating all the fields manifest. We will use this example to illustrate all our discussions.

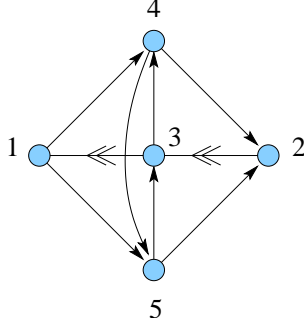


Figure 1: Quiver diagram for Model II of dP_2 .

In [34], it was realized that all the information in the quiver diagram and the superpotential of a toric phase can be encapsulated in a single object: the **periodic quiver**. A periodic quiver is a planar quiver drawn on the surface of a 2-torus (equivalently, a doubly periodic infinite quiver on the plane) s. t. every plaquette corresponds to a term in the superpotential. The sign of the superpotential terms is given by the orientation of the corresponding plaquettes, which alternates between clockwise and counterclockwise. The toric condition is automatically incorporated in the periodic quiver, since every field appears precisely in two neighboring plaquettes with opposite orientation.

It has been conjectured that any quiver corresponding to D3-branes probing non-compact, toric Calabi–Yau threefolds can be embedded in a T^2 [34]. Furthermore, the two cycles around the T^2 have been identified with the non-R symmetry $U(1)$ isometries [43]. In Section 2.1, we discuss how conformal invariance restricts the possible embeddings of the periodic quiver. Figure 2 shows the periodic quiver for our dP_2 example.

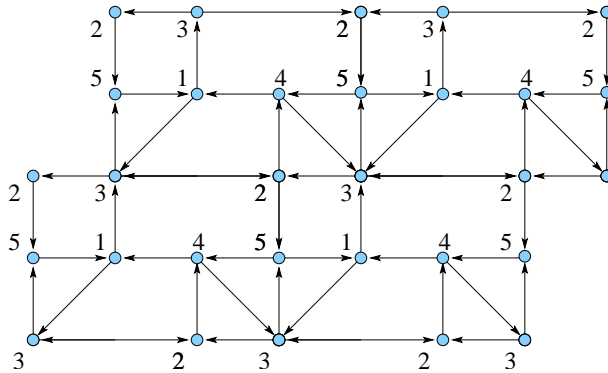


Figure 2: Periodic quiver for Model II of dP_2 . We show several fundamental cells.

Along the rest of the paper, our working hypothesis will be that *we consider gauge theories that are described by periodic quivers on T^2* . For this class of theories, we will show that the GLSM determination of the moduli space can be translated into a dimer problem.

The superpotential can be written schematically as

$$W = \sum_{\mu} \pm W_{\mu} \quad (2.2)$$

where every superpotential term W_{μ} is a gauge invariant mesonic operator with R-charge equal to 2 and neutral under the $U(1) \times U(1)$ flavor symmetry¹. We have explicitly indicated the sign of each term, which satisfy the toric condition.

In toric quivers, F-term equations can be used to show that all these operators are equivalent in the chiral ring. The toric condition implies that every field X_i appears (linearly) in exactly two superpotential terms. Let us call them W_1 and $-W_2$ (according to the toric condition both contributions have opposite signs). Then

$$0 = X \partial_X W = X \partial_X (W_1 - W_2) = W_1 - W_2 \quad (2.3)$$

This becomes very intuitive from the perspective of the periodic quiver (see Figure 3), where one can show that any two adjacent plaquettes are equal by using the F-term relation for the common field. Iterating this process we see that, once F-term equations are taken into account, all superpotential terms are identical. This idea has already been used in [43].

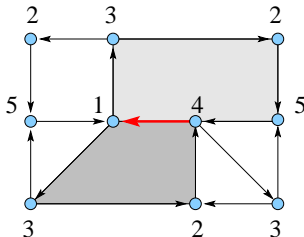


Figure 3: Two plaquettes are equal once the F-term equation for the common field is imposed.

In [34], an alternative representation of the gauge theory, dubbed **brane tiling**² was introduced. The brane tiling is constructed by dualizing the periodic quiver graph: Nodes, arrows and plaquettes of the periodic quiver are replaced by faces, transverse lines and nodes, respectively.

¹In some cases the $U(1)^2$ global symmetry can be enhanced. For example, for $Y^{p,q}$ theories the flavor symmetry is $SU(2) \times U(1)$ [11].

²We alert the reader that the goal of this paper is independent of the possible interpretation of the tiling as a physical object, such as a configuration of branes. However, we will adhere to the term **brane tiling** for simplicity. The arguments that identify brane tilings with physical configurations of D5- and NS5-branes are primarily based on the analogy with brane box and brane diamond constructions dual to orbifold singularities [44, 45, 46]. A concrete string theory realization of the tiling was studied in detail in [36].

The resulting tiling is a **bipartite graph**. This means that it is possible to assign nodes two colors (by convention we choose black and white) such that white nodes are only connected to black nodes and viceversa. The coloring of nodes is in one-to-one correspondence with the orientation of plaquettes in the periodic quiver (hence the sign of superpotential terms). Edges in the tiling carry a natural orientation (for example from white to black nodes), which corresponds to the orientation of arrows in the periodic quiver.

We can translate among periodic quiver, brane tiling and gauge theory concepts using the following dictionary

Periodic quiver	Brane tiling	Gauge theory
node	face	$SU(N)$ gauge group
arrow	edge	bifundamental (or adjoint)
plaquette	node	superpotential term

We denote F , E and N the number of faces, edges and nodes in the tiling. They correspond to the number of gauge groups, chiral multiplets and superpotential terms in the gauge theory.

For a comprehensive description of brane tilings we refer the reader to [34]. Figure 4 shows the brane tiling for the dP_2 example under consideration, obtained by dualizing the periodic quiver in Figure 2

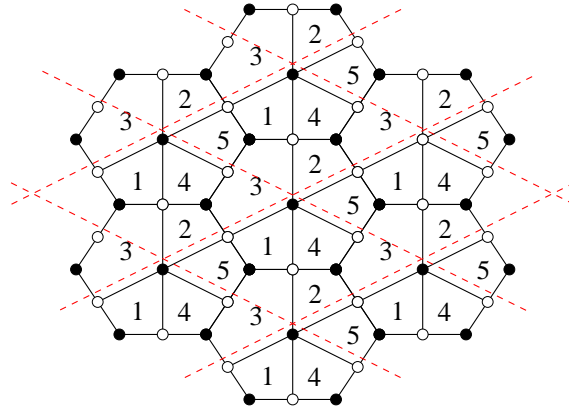


Figure 4: Brane tiling for Model II of dP_2 .

In analogy to the chemical terminology, every edge in the tiling is denoted a **dimer**. A **perfect matching** is a collection of edges (dimers) such that every node in the tiling is the endpoint of exactly one edge in the set. For later reference, we list all perfect matchings for the dP_2 brane tiling in the Appendix. Perfect matchings play a fundamental role in our forthcoming discussion.

2.1 Geometry of the tiling embedding from conformal invariance

In the previous section we stated that we will focus on tilings of a two dimensional torus. Since the gauge theories under consideration have a finite number of gauge groups, fields and superpotential terms, it is natural to represent them by a tiling of a **compact** Riemann surface Σ . But, is any Σ a valid option? Why do we choose a T^2 ? Interestingly, as we discuss in this section, the gauge theory actually constraints the geometry of Σ .

Conformal invariance at the IR fixed point requires the beta functions for all superpotential and gauge couplings to be zero. For superpotential couplings this implies that

$$\sum_{\substack{i \in \text{edges} \\ \text{around node}}} R_i = 2 \quad \text{for every node} \quad (2.4)$$

while vanishing of gauge coupling beta functions corresponds to

$$2 + \sum_{\substack{i \in \text{edges} \\ \text{around face}}} (R_i - 1) = 0 \quad \text{for every face} \quad (2.5)$$

Adding (2.5) over all faces and using (2.4) we conclude that

$$F + N - E = \chi(\Sigma) = 0 \quad (2.6)$$

Hence, conformal invariance implies that the Euler characteristic of Σ has to be zero. This fact has been already noticed in [34]. There are only two options for Σ . On one hand, it can be a T^2 as considered so far in the paper and in the literature. On the other hand, there is the interesting possibility of Σ being the Klein Bottle. Figure 5 shows an example of a bipartite tiling of the Klein Bottle. This tiling is known as the Franklin graph [47] and has $F = 6$, $N = 12$ and $E = 18$, hence satisfying (2.6).

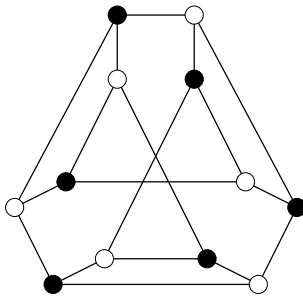


Figure 5: A bipartite graph tiling the Klein Bottle.

At present, both the gauge theory and geometric interpretations of such a tiling are unknown and remain an intriguing question that deserves further study. Along the rest of the paper, we

will restrict ourselves to the case in which $\Sigma = T^2$. The planar quiver, dual to the tiling, will consequently be also embedded in a T^2 .

2.2 Height function

Given a perfect matching M , it is possible to define an integer-valued **height function** h over the brane tiling [48, 49]. In order to do so we fix a reference perfect matching M_0 and a face f_0 . The difference $M - M_0$ defines a set of closed curves over the tiling. The minus sign flips the orientation of bifundamentals associated with the edges of M_0 , giving the resulting closed curves a definite orientation. The height function jumps by ± 1 when crossing a curve, where the sign is given by the orientation of the crossing. The height for f_0 is set to be zero. Notice that the difference of the height functions of two matchings is well-defined independently of M_0 .

The **slope** of a perfect matching is defined as the height change (h_x, h_y) when moving from one unit cell to the next one along the two fundamental directions. Changing M_0 amounts to a constant shift (h_{x0}, h_{y0}) in the slopes of all perfect matchings.

We exemplify the concepts presented in this section with dP_2 . Figure 6 shows a perfect matching, a reference perfect matching and the corresponding height function. In this case, we see that the slope is $(h_x, h_y) = (-1, 0)$.

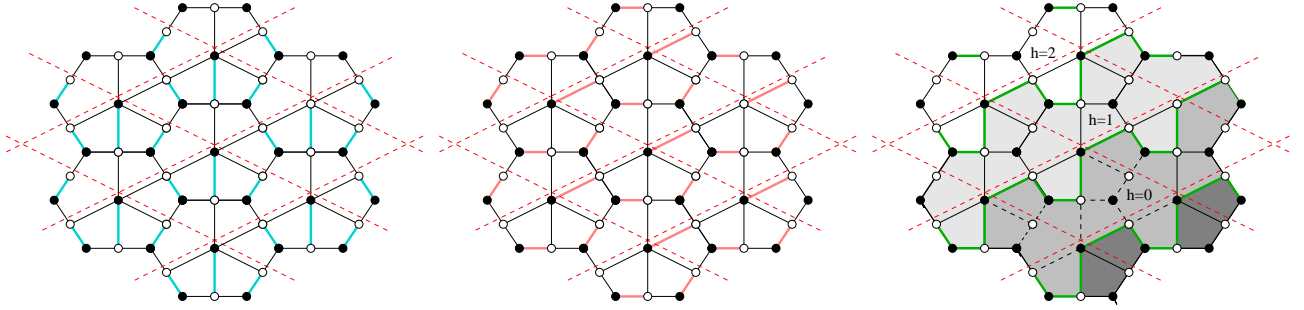


Figure 6: (a) The dimers in the a perfect matching M are shown in cyan. (b) The dimers in the reference perfect matching M_0 are shown in red. (c) The height function, whose level curves are given by $M - M_0$.

There is an equivalent way to define slopes, that later will turn out to be useful. To every perfect matching we can associate a **unit flow** on its edges, directed from white to black nodes. The slope then corresponds to the net flux between adjacent fundamental regions in the x and y directions. The Appendix gives the slopes for all perfect matchings of Model II of dP_2 . We will come back to the interpretation of matchings as unit flows in Section 5.2.

It is straightforward to count the number of perfect matchings with a given slope [48, 49]. In order to do so, we first introduce the Kasteleyn matrix of the tiling $K(x, y)$. It is a weighted, signed, $(N/2) \times (N/2)$ adjacency matrix defined as follows. In our convention, the rows of $K(x, y)$ are indexed by white nodes and its columns by black nodes. We associate a ± 1 weight to every edge e_i in the tiling such that when we multiply the weights around every face we have

$$\text{sign} \left(\prod e_i \right) = \begin{cases} +1 & \text{if } (\# \text{ edges}) = 2 \pmod{4} \\ -1 & \text{if } (\# \text{ edges}) = 0 \pmod{4} \end{cases} \quad (2.7)$$

Next we take two fundamental paths \mathcal{C}_x and \mathcal{C}_y in the graph dual to the brane tiling winding once around the $(1,0)$ and $(0,1)$ cycles of the 2-torus. These paths are conventionally denoted **flux lines** and can be visualized as the boundaries of the fundamental region. The weight of every edge in the tiling that is crossed by \mathcal{C}_x is then multiplied by x or x^{-1} depending on the orientation of the crossing. Respectively, edges crossed by \mathcal{C}_y are multiplied by y or y^{-1} .

The determinant of the Kasteleyn matrix $P(x,y) = \det K(x,y)$ is a Laurent polynomial, the so-called **characteristic polynomial** of the dimer model. It has the following general form

$$P(x,y) = x^{h_{x0}} y^{h_{y0}} \sum c_{h_x, h_y} x^{h_x} y^{h_y} \quad (2.8)$$

$P(x,y)$ is the partition function of perfect matchings on the brane tiling, in the sense that the integer coefficients $|c_{h_x, h_y}|$ count the number of perfect matchings with slope (h_x, h_y) [49].

In our example, we have

$$K = \begin{pmatrix} 1 - x^{-1} & y & 1 \\ 1 & 1 & x \\ -1 + x^{-1}y^{-1} & 1 & 1 \end{pmatrix} \quad (2.9)$$

Then

$$P(x,y) = x^{-1}y^{-1} - x^{-1} + 5 - x - y - xy \quad (2.10)$$

which gives the following counting of perfect matchings

slope	# matchings
(-1,-1)	1
(-1,0)	1
(0,0)	5
(1,0)	1
(0,1)	1
(1,1)	1

that is in precise agreement with the direct counting in the Appendix.

3. Toric geometry from gauge theory

We now review the procedure for computing the moduli space of a given toric quiver (i.e. quiver plus toric superpotential). For N D3-brane probes, the moduli space along the mesonic branch corresponds to the symmetric product of N copies of the probed geometry. This procedure has been algorithmized in [24] and dubbed the Forward Algorithm. It involves the following steps:

- Use F-flatness equations to express the fields in the quiver (which transform in bifundamental or adjoint representations) X_i , $i = 1, \dots, E$ in terms of $F + 2$ independent variables v_j . Although the v_j 's can be taken to be a subset of the X_i fields, other choices are also possible. For example, as we will discuss later, dimers pick other combinations which turn out to be more natural. The final answer does not depend on this choice. Since for toric quivers the F-term equations are of the form *monomial* = *monomial*, each X_i is given by a product of v_j 's to appropriate powers. This can be encoded in an $E \times (F + 2)$ matrix K according to

$$X_i = \prod_j v_j^{K_{ij}}, \quad i = 1, \dots, E, \quad j = 1, \dots, F + 2 \quad (3.1)$$

The X_i can involve negative powers of the v_j 's, i.e. K_{ij} may have negative entries. The row vectors \vec{K}_i of K span a cone M_+ in \mathbb{R}^{F+2} , corresponding to non-negative linear combinations of them.

- Next, to get rid of the negative powers, we introduce new variables p_α , $\alpha = 1, \dots, N_\sigma$. In order to do so, we compute the cone N_+ dual to M_+ . N_+ is spanned by vectors \vec{T}_α , such that $\vec{K}_i \cdot \vec{T}_\alpha \geq 0$. These vectors can be organized as the columns of an $(F + 2) \times N_\sigma$ integer matrix T such that $K \cdot T \geq 0$ for all entries. The dimension of the dual cone N_σ is not known a priori and is determined by explicitly computing N_+ . The intermediate and original variables v_j and X_i are expressed in terms of the p_α as follow

$$v_j = \prod_\alpha p_\alpha^{T_{j\alpha}} \quad X_i = \prod_\alpha p_\alpha^{\sum_j K_{ij} T_{j\alpha}} \quad (3.2)$$

The amount of operations required to compute N_σ grows with the size of the gauge theory. This growth becomes prohibitive when trying to apply the Forward Algorithm to gauge theories with large quivers. Later, we will explain how this difficulty is circumvented by the dimer model.

- A convenient way to encode the relations among the N_σ variables p_α and the original $F + 2$ v_j is by obtaining them as D-terms of an appropriately chosen $U(1)^{N_\sigma - (F+2)}$ gauge group. Its action is given by an $(N_\sigma - F - 2) \times N_\sigma$ charge matrix Q_F (where the subindex F indicates that Q_F contains all the information about F-term equations). Gauge invariance of the v_j 's under the new gauge group gives rise to the desired relations. Hence, Q_F is such that

$$T \cdot Q_F^T = 0 \quad (3.3)$$

- The charges of fields under the F gauge groups of the quiver are summarized by the $F \times E$ **incidence matrix** d . It is defined as $d_{li} = \delta_{l, \text{head}(X_i)} - \delta_{l, \text{tail}(X_i)}$. Every column associated to a bifundamental field contains a 1 and a -1 and the rest of the entries are 0's. Adjoint fields are represented in quiver language by arrows starting from and ending at the same

node. Hence, the corresponding columns have all 0's. It is clear that one of the rows of d is redundant. Thus, we define the matrix $(F - 1) \times E$ matrix Δ , which is obtained from d by deleting one of its rows. For our example, we have

$$\Delta = \left[\begin{array}{c|cccccccccccc} & X_{14} & X_{31} & X_{15} & Y_{31} & X_{23} & X_{52} & Y_{23} & X_{42} & X_{34} & X_{53} & X_{45} \\ \hline 1 & -1 & 1 & -1 & 1 & 0 & 0 & 0 & 0 & 0 & 0 & 0 \\ 2 & 0 & 0 & 0 & 0 & -1 & 1 & -1 & 1 & 0 & 0 & 0 \\ 3 & 0 & -1 & 0 & -1 & 1 & 0 & 1 & 0 & -1 & 1 & 0 \\ 4 & 1 & 0 & 0 & 0 & 0 & 0 & 0 & -1 & 1 & 0 & -1 \end{array} \right] \quad (3.4)$$

The $F - 1$ independent D-term equations of the original theory are implemented by adding a $U(1)^{F-1}$ gauge symmetry to the GLSM. The charges of the p_α under these symmetries is given by an $(F - 1) \times N_\sigma$ matrix Q_D which can be determined in two steps. First, we construct an $(F - 1) \times (F + 2)$ matrix V that translates the charges of the X_i 's to those of the v_j 's. Thus,

$$V \cdot K^T = \Delta \quad (3.5)$$

Next, we find an $(F + 2) \times N_\sigma$ matrix U that transform the charges of v_j 's into those of the p_α 's

$$U \cdot T^T = \text{Id}_{(F+2) \times (F+2)} \quad (3.6)$$

Finally, we have

$$Q_D = V \cdot U \quad (3.7)$$

Q_D and Q_F are combined into a single $(N_\sigma - 2) \times N_\sigma$ charge matrix Q

$$Q = \begin{pmatrix} Q_D \\ Q_F \end{pmatrix} \quad (3.8)$$

The construction we outlined can be interpreted as a Witten's two dimensional **gauged linear sigma model** (GLSM) of N_σ chiral fields p_α and $U(1)^{N_\sigma-3}$ gauge group with charges given by Q .

- The $U(1)$ charges defined above are exactly those that appear in the construction of a toric variety as a symplectic quotient. In toric geometry it is standard to encode the charge matrix by means of a **toric diagram**.

$$G = (\text{Ker}(Q))^T \quad (3.9)$$

One of the rows in G can be set to have all entries equal to 1 by an appropriate $SL(3, \mathbb{Z})$ transformation. This is the Calabi-Yau condition and amounts to the fact that the sum of the charges of all the p_α under any of the $U(1)$ gauge symmetries is zero. Effectively, we are

left with a two dimensional toric diagram. Every GLSM field p_α corresponds to a point in the toric diagram, which is a vector \vec{v}_α in \mathbb{Z}^3 . Q is given by linear relations of the form

$$\sum_{i=1}^n Q_a^\alpha \vec{v}_\alpha = 0 \quad (3.10)$$

satisfied by the \vec{v}_α 's.

Figure 7 summarizes the relevant matrices in the Forward Algorithm.

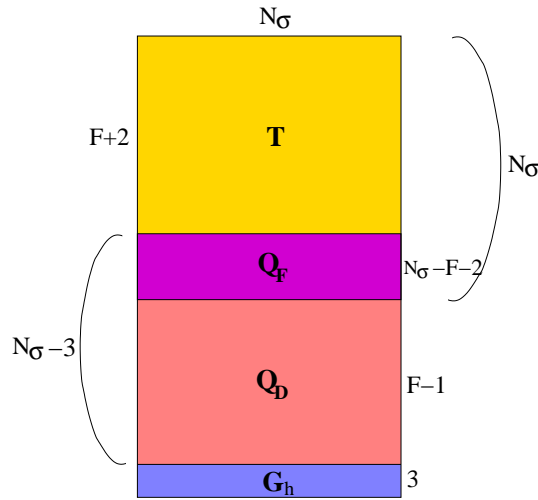


Figure 7: Relevant matrices in the Forward Algorithm.

4. The conjecture

Having introduced all necessary concepts, we are ready to study the conjecture of [34]. It is convenient to divide the conjecture into two parts, to which we refer as the **Mathematical** and the **Physical Dimer Conjectures**.

Mathematical dimer conjecture

The mathematical dimer conjecture states that there is a one-to-one correspondence between fields p_α in the gauged linear sigma model construction of the toric moduli space of the given toric gauge theory and perfect matchings in the brane tiling dual to the toric quiver. Here, when we refer to a toric gauge theory we mean a gauge theory whose quiver can be drawn on a surface of a 2-torus, s. t. the plaquettes give the terms in the superpotential (see discussion in Section

2.1). Furthermore, according to the conjecture, the toric diagram is the Newton polygon of the characteristic polynomial (i.e. the set of integer exponents of monomials [49]) which, as we have already discussed, is the set of height function monodromies (“slopes”) of the perfect matchings.

Physical dimer conjecture

The physical dimer conjecture identifies dimers and tilings with physical objects. According to the conjecture, the brane tiling is interpreted as a physical brane configuration. It consists of an NS5-brane extended in the 0123 directions that wraps an holomorphic curve in 4567. The 5 and 6 directions are periodically identified giving rise to the 2-torus. D5-branes extend in 012346, suspended within the “holes” of the NS5-brane in the 46 torus. Every stack of D5-branes gives rise to a gauge group. Strings crossing every NS5-brane segment and connecting two D5-brane stacks correspond to chiral multiplets transforming in the bifundamental representation of the corresponding gauge groups. Gauge invariant superpotential terms are produced by the coupling of massless string states at the nodes of the NS5-brane configuration. This configuration is conjectured to be related to the D3-branes over the singularity by two T-dualities. The suspended D5-branes are dual to the probe D3-branes and the NS5-brane structure is dual to the singular geometry.

The correspondence between dimers and a physical brane system could be more subtle and might differ from the one suggested by the physical dimer conjecture. However, the validity of the mathematical dimer conjecture, which is the main subject of this paper, is completely independent of how tilings are realized in terms of branes³.

Having introduced the conjectures of [34], we devote the rest of the paper to proving the mathematical dimer conjecture.

5. The proof

In this section we prove the Mathematical Dimer Conjecture. As we said before, we prove it for toric gauge theories whose quivers (and hence their brane tilings) are embedded in a two-torus. A considerable amount of evidence supporting its validity has been accumulated in the literature. This includes:

³Recently, another physical description of the tiling has been developed in [36]. Using mirror symmetry, the D3-branes are mapped to a system of D6-branes that wraps a self-intersecting T^3 torus. The mirror geometry is a double fibration over the complex W plane, one being the $W = uv$ torus fibration degenerating at the origin and another being the $W = P(w, z)$ fibration degenerating at some critical points. Here $P(w, z) \equiv \det(\text{Kasteleyn})$ is the spectral curve with $(w, z) = (e^{s+i\theta}, e^{t+i\phi}) \in (\mathbb{C}^*)^2$. The spectral curve can then be projected to the non-compact space (s, t) which yields the amoeba whose spine is the pq-web of the toric diagram. Projection on the compact (θ, ϕ) coordinates gives the so-called alga of the curve. Its skeleton is the rhombus loop diagram that has been used to construct the brane tiling for a given toric diagram [35, 36]. This construction supports the D5–NS5 tiling proposal of [34], which appears when T-dualizing along the S^1 fibre in the uv plane.

- Construction of the correct toric diagram for the moduli space of gauge theories for an infinite number of singularities. This number is infinite thanks to the determination of the tilings for the $Y^{p,q}$ [34] and $L^{a,b,c}$ manifolds [15, 17].
- Precise agreement between the number of perfect matchings and the multiplicity of GLSM fields in toric diagrams for various models [15].
- Derivation of Seiberg dual theories by transformations of the tilings preserving the Newton polygon of the characteristic polynomial [15, 35].
- In [15], it was shown that given a simple proposal to express quiver fields in terms of perfect matchings, F-term conditions are straightforwardly satisfied. This proposal will be derived as part of our proof.
- The geometry of brane tilings has recently been investigated in [36]. The results of this paper show how tilings appear in the description of toric gauge theories by explicitly deriving them from the mirror geometry but do not prove the correspondence between perfect matchings and GLSM fields.

Our computations with dimers will closely follow those of the Forward Algorithm. It is important to keep in mind that some of the steps (or intermediate matrices) are naturally skipped by the inherent simplifications of the dimer approach. In order to avoid confusion we will use tilded variables at some stages of the proof. In the end, we will show that they can be identified with the untilded ones of the Forward Algorithm.

5.1 Solving F-term conditions: gauge transformations and magnetic coordinates

The tiling is bipartite, therefore each edge has a natural orientation from its white vertex to its black vertex. Any weight function $\epsilon(e)$ on the edges defines a 1-form, satisfying $\epsilon(-e) = -\epsilon(e)$, where $-e$ is the edge with opposite direction [49]. We denote the linear space of 1-forms on the tiling by Ω^1 . Analogously, the functions on nodes and faces define 0- and 2-forms in Ω^0 and Ω^2 . The three spaces are related by differentials

$$0 \rightarrow \Omega^0 \xrightarrow{d} \Omega^1 \xrightarrow{d} \Omega^2 \rightarrow 0 \quad (5.1)$$

We can now define **gauge transformations** on the tiling, whose action on the 1-forms is given by [49]

$$\epsilon'(e_i) = \epsilon(e_i) + df \quad f \in \Omega^0 \quad (5.2)$$

That is

$$\epsilon'(e_i) = \epsilon(e_i) + f(\mathbf{b}_i) - f(\mathbf{w}_i) \quad (5.3)$$

with \mathbf{b}_i and \mathbf{w}_i the black and white nodes at the endpoints of edge e_i . These gauge transformations of the tiling should not be confused with the gauge symmetries of the quiver theory. We are confident that the distinction between both types of gauge transformations will be clear from the context in which we use them. Given a closed path on the tiling

$$\gamma = \{\mathbf{w}_0, \mathbf{b}_0, \mathbf{w}_1, \mathbf{b}_1, \dots, \mathbf{b}_{k-1}, \mathbf{w}_k\} \quad \mathbf{w}_k = \mathbf{w}_0 \quad (5.4)$$

we define the **magnetic flux** through γ as

$$B(\gamma) = \int_{\gamma} \epsilon = \sum_{i=1}^{k-1} [\epsilon(\mathbf{w}_i, \mathbf{b}_i) - \epsilon(\mathbf{w}_{i+1}, \mathbf{b}_i)] \quad (5.5)$$

Magnetic fluxes are clearly gauge invariant. The brane tiling is embedded in a two dimensional torus. Hence, gauge inequivalent classes of 1-forms are parameterized by $\mathbb{R}^{F-1} \oplus \mathbb{R}^2$. The first term corresponds to $d\epsilon \in \Omega^2$, a function on the faces of the tiling subject to the condition $\sum d\epsilon = 0$. We can specify the \mathbb{R}^{F-1} part by the magnetic fluxes $B_z(j)$ ($j = 1, \dots, F-1$) through the γ_i contours around $F-1$ faces. The remaining two parameters (B_x, B_y) correspond to fluxes around two non-trivial cycles (γ_x, γ_y) winding around the torus.

Gauge transformations are of particular interest because taking ϵ to be the energy function they do not modify the energy difference between perfect matchings. Hence, the probability distribution of perfect matchings is invariant under gauge transformations.

In this section, we will exploit gauge transformations with a different goal, namely to provide a convenient set of variables (mostly in Ω^2) that solve the F-term equations. For this purpose, we define the complex 1-form

$$\epsilon(e_i) = \ln X_i \quad \Rightarrow \quad \text{under gauge transformations: } X'_i = X_i e^{f(\mathbf{b}_i) - f(\mathbf{w}_i)} \quad (5.6)$$

In this context, we refer to the X_i 's as **weights**⁴.

Using (5.6), we can define new variables associated to closed paths

$$\tilde{v}(\gamma) = e^{\int_{\gamma} \epsilon} = \prod_{i=1}^{k-1} \frac{X(\mathbf{w}_i, \mathbf{b}_i)}{X(\mathbf{w}_{i+1}, \mathbf{b}_i)} \quad (5.7)$$

where the product runs over the contour γ . Then $\{\tilde{v}_j \equiv \tilde{v}(\gamma_j), \tilde{v}_x, \tilde{v}_y\}$ provides a parametrization of inequivalent gauge classes.

We define a convenient basis of 0-forms $F^{(\mu)}$, $\mu = 1, \dots, N$,

$$F^{(\mu)} \quad \begin{cases} f_{\mu} = 1 \\ f_{\nu} = 0 \text{ for } \nu \neq \mu \end{cases} \quad (5.8)$$

⁴If we regard $-\epsilon(e_i)$ as the energy of a link, the X_i 's can be interpreted as complex valued Boltzmann weights.

Their virtue is that superpotential terms transform simply under the corresponding gauge transformations. Taking the gauge transformation for $\alpha_\mu F^{(\mu)}$, with α_μ a complex coefficient, we get

$$W'_\mu = W_\mu e^{\text{sign}(\mu) v_\mu \alpha_\mu} \quad (5.9)$$

where v_μ is the valence of node μ (i.e. the order of the associated superpotential term W_μ) and following (5.6) $\text{sign}(\mu)$ is 1 for black nodes and -1 for white nodes.

As discussed in Section 2, solving F-term conditions corresponds to setting all the W_μ 's equal. Given arbitrary values of the W_μ , it is possible to set them equal to W_1 by the basic gauge transformations of (5.9) with

$$\alpha_\mu = \frac{\text{sign}(\mu)}{v_\mu} \frac{\ln W_1}{\ln W_\mu} \quad (5.10)$$

In other words, solving F-term equations corresponds in this language to **partially fixing the gauge**. Each gauge choice can be labeled by the common value of $W_\mu = W_1$ ⁵. Equivalently, one can label gauge choices using the more symmetric variable \mathcal{V} defined as

$$\mathcal{V} = W_1^N = \prod_{\mu=1}^N W_\mu = \prod_{i=1}^E X_i^2 \quad (5.11)$$

We denote \mathcal{V} , the \tilde{v}_j 's, \tilde{v}_x and \tilde{v}_y the **flux variables**.

We have just seen that on each gauge orbit there exists a unique solution to F-term equations for every value of \mathcal{V} . Hence, we conclude that *solutions to F-flatness equations are parametrized by the $F+2$ flux variables: the value of \mathcal{V} indicating a partial gauge fixing, along with the variables \tilde{v}_j ($j = 1, \dots, F-1$), \tilde{v}_x and \tilde{v}_y parametrizing gauge equivalence classes*. It is now clear that these fluxes can be identified with the v_j ($j = 1, \dots, F+2$) variables of the Forward Algorithm.

With this identification, it is straightforward to write down a left inverse matrix for K , which we call K_L^{-1} . This is an $(F+2) \times E$ matrix such that $K_L^{-1} K = \text{Id}_{(F+2) \times (F+2)}$.

For our dP_2 example, we have

$$K_L^{-1} = \begin{array}{c|cccccccccccc} & X_{14} & X_{31} & X_{15} & Y_{31} & X_{23} & X_{52} & Y_{23} & X_{42} & X_{34} & X_{53} & X_{45} \\ \hline \tilde{v}_1 & 1 & -1 & 1 & -1 & 0 & 0 & 0 & 0 & 0 & 0 & 0 \\ \tilde{v}_2 & 0 & 0 & 0 & 0 & 1 & -1 & 1 & -1 & 0 & 0 & 0 \\ \tilde{v}_3 & 0 & 1 & 0 & 1 & -1 & 0 & -1 & 0 & 1 & -1 & 0 \\ \tilde{v}_4 & -1 & 0 & 0 & 0 & 0 & 0 & 0 & 1 & -1 & 0 & 1 \\ \hline \tilde{v}_x & -1 & 0 & 0 & 1 & -1 & 0 & 0 & 1 & 0 & 0 & 0 \\ \tilde{v}_y & 1 & -1 & 0 & 0 & 0 & 0 & 0 & 0 & 0 & 1 & -1 \\ \hline \mathcal{V} & 2 & 2 & 2 & 2 & 2 & 2 & 2 & 2 & 2 & 2 & 2 \end{array} \quad (5.12)$$

for which we have taken the γ_i loops to run clockwise around faces, and γ_x and γ_y are the two non-trivial cycles shown in Figure 8, i.e.

⁵We thank Alastair King for discussions on related ideas.

$$\begin{aligned}\tilde{v}_x &= X_{14}^{-1} X_{42} X_{23}^{-1} Y_{31} \\ \tilde{v}_y &= X_{53} X_{31}^{-1} X_{14} X_{45}^{-1}\end{aligned}\tag{5.13}$$

With this choice of contours, it is clear that the first $F - 1$ rows of K_L^{-1} are equal to $-\Delta$ (see (3.4)). There are other paths equivalent to γ_x and γ_y that are obtained by deforming them using F-term equations.

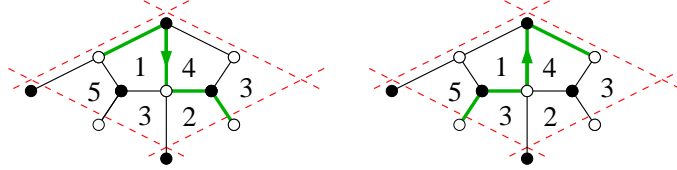


Figure 8: Contours defining \tilde{v}_x and \tilde{v}_y .

The matrix K converts magnetic variables into weight variables. We do not determine K explicitly in this section as it is not necessary for our discussion. As explained in Section 3, the vectors \vec{n}_i corresponding to rows in K ($i = 1, \dots, E$) span a cone \mathcal{S} in \mathbb{R}^{F+2} .

5.2 The GLSM fields are perfect matchings

In the previous section we discussed at length how the F-flatness conditions can be satisfied in terms of the \tilde{v}_i magnetic fluxes that are in one-to-one correspondence with the variables v_j according to (5.7). The relation between these variables and the original X_i fields are encoded in the matrix K , whose rows span the cone M_+ in \mathbb{R}^{F+2} . The Forward Algorithm proceeds by computing the cone dual to M_+ :

$$N_+ = \{x \in \mathbb{R}^{F+2} \mid \langle \vec{K}_i, x \rangle \geq 0 \text{ for } i = 0, \dots, E\}\tag{5.14}$$

There are N_σ spanning vectors for this dual cone N_+ . These N_σ vectors define the columns \vec{T}_j of the matrix T and they are in one-to-one correspondence with the homogeneous p_α GLSM coordinates.

We would like to understand the computation of the dual cone in terms of tiling techniques. In order to do so, we introduce a slightly different viewpoint that will prove to be useful.

An arbitrary real weight system on the edges can be interpreted as a **white-to-black flow**⁶ [49]. The (possibly negative) strength of the flow from white to black node along an edge e_i is given by the corresponding real weight c_i . The real weights considered in this section are not to be confused with the complex weights given by X_i that we have discussed earlier.

A flow is nonnegative if it has a nonnegative strength on all edges of the tiling ($c_i > 0$ for all e_i). The flows are typically not divergence free, therefore there can be sinks and sources at the vertices.

⁶The flow space should not be confused with the flux space, which was introduced in the previous section and is \mathbb{R}^{F+2} .

The net flux coming out of a given white node or into a black node is denoted the **vorticity** of the node.

For each point in flux space $x \in \mathbb{R}^{F+2}$ we define a real flow on the tiling whose strength at the i^{th} edge is given by $\sum_j K_{ij}x_j$. Hence the points inside N_+ correspond to nonnegative flows in this picture.

We want to find the spanning vectors \vec{T}_α of the dual cone $N_+ \in \mathbb{R}^{N_F+2}$. Following our discussion in Section 5.1, we can rescale the vectors \vec{T}_α by a positive real number using the gauge transformations of the dimer model. Thus we can set their vorticity to one. Therefore, we can focus on the hyperplane $H \subset \mathbb{R}^{N_F+2}$ such there is a unit source residing at every white vertex and a unit sink at the black ones. The flows associated with this hyperplane are called **unit flows**.

The vectors \vec{T}_α span the cone N_+ , hence they also span the intersection $H \cap N_+$ in flux space. From the previous discussion, we know that this intersection is linearly mapped by K_{ij} to nonnegative unit flows $P \subset \mathbb{R}^E$ in flow space. It is well-known in the literature that the set of nonnegative unit flows is a convex polytope in the flow space and that perfect matchings are vertices of this polytope (Perfect Matching Polytope Theorem, [50]). Their preimages are the spanning vectors \vec{T}_α in flux space. For \vec{T}_α , the flow on the i^{th} edge is given by $\sum_j K_{ij}(\vec{T}_\alpha)_j = \sum_j K_{ij}T_{j\alpha}$. We conclude that there is a one-to-one correspondence between the GLSM fields in the Forward Algorithm and perfect matchings.

Perfect matchings are naturally represented as unit flows, hence they immediately determine KT . By introducing the following “product” between perfect matchings and edges in the tiling

$$\langle e_i, p_\alpha \rangle = \begin{cases} 1 & \text{if } e_i \in p_\alpha \\ 0 & \text{if } e_i \notin p_\alpha \end{cases} \quad (5.15)$$

the matrix KT is simply

$$(KT)_{i\alpha} = \langle e_i, p_\alpha \rangle \quad (5.16)$$

The correspondence between GLSM fields and perfect matchings and the computation of KT in terms of perfect matchings that we derived in this section was originally proposed in [34].

Using (5.16) for dP_2 , we have

$$KT^T = \begin{array}{c|cccccccccccc} & X_{14} & X_{31} & X_{15} & Y_{31} & X_{23} & X_{52} & Y_{23} & X_{42} & X_{34} & X_{53} & X_{45} \\ \hline p_1 & 0 & 1 & 0 & 1 & 0 & 0 & 0 & 0 & 1 & 0 & 0 \\ p_2 & 0 & 0 & 1 & 0 & 0 & 0 & 0 & 1 & 0 & 0 & 1 \\ p_3 & 0 & 0 & 0 & 0 & 0 & 1 & 0 & 1 & 0 & 1 & 0 \\ p_4 & 0 & 0 & 0 & 0 & 1 & 0 & 1 & 0 & 0 & 1 & 0 \\ p_5 & 1 & 0 & 1 & 0 & 0 & 0 & 0 & 0 & 1 & 0 & 0 \\ p_6 & 0 & 0 & 0 & 1 & 0 & 0 & 0 & 1 & 0 & 1 & 0 \\ p_7 & 1 & 0 & 0 & 0 & 1 & 0 & 0 & 0 & 0 & 1 & 0 \\ p_8 & 0 & 1 & 0 & 0 & 1 & 0 & 0 & 0 & 0 & 0 & 1 \\ p_9 & 0 & 0 & 1 & 0 & 0 & 0 & 1 & 0 & 1 & 0 & 0 \\ p_{10} & 0 & 1 & 0 & 0 & 0 & 1 & 0 & 0 & 1 & 0 & 0 \end{array} \quad (5.17)$$

As we discussed in the previous section, the left inverse of K , which we called K_L^{-1} , arises naturally using dimer methods. Then, it is straightforward to write down

$$T = K_L^{-1} K T \quad (5.18)$$

$$T = \begin{array}{c|cccccccccc} & p_1 & p_2 & p_3 & p_4 & p_5 & p_6 & p_7 & p_8 & p_9 & p_{10} \\ \hline \tilde{v}_1 & -2 & 1 & 0 & 0 & 2 & -1 & 1 & -1 & 1 & -1 \\ \tilde{v}_2 & 0 & -1 & -2 & 2 & 0 & -1 & 1 & 1 & 1 & -1 \\ \tilde{v}_3 & 3 & 0 & -1 & -3 & 1 & 0 & -2 & 0 & 0 & 2 \\ \tilde{v}_4 & -1 & 2 & 1 & 0 & -2 & 1 & -1 & 1 & -1 & -1 \\ \hline \tilde{v}_x & 1 & 1 & 1 & -1 & -1 & 2 & -2 & -1 & 0 & 0 \\ \tilde{v}_y & -1 & -1 & 1 & 1 & 1 & 1 & 2 & -2 & 0 & -1 \\ \hline \mathcal{V} & 6 & 6 & 6 & 6 & 6 & 6 & 6 & 6 & 6 & 6 \end{array} \quad (5.19)$$

Notice that the fact that T may have negative entries is not a problem. The important point is that $(KT)_{i\alpha} \geq 0$. In fact we can give a straightforward definition of T in terms of the tiling, similar to (5.16). In order to do so, we take into account the edges e_i in the curves γ_j that define the magnetic fluxes (similarly, all e_i 's are included for \mathcal{V}). The γ_j 's have an **orientation** and then the fields X_i associated to edges e_i appear with a ± 1 power that we denote $\text{sign}(e_i)$. Combining these ideas, we get

$$T_{j\alpha} = \sum_{e_i \in \gamma_j} \text{sign}(e_i) \langle e_i, p_\alpha \rangle \quad (5.20)$$

5.3 Height changes as positions in a toric diagram

So far we have shown that GLSM fields are perfect matchings. This is half of the proof of the Mathematical Dimer Conjecture, which in addition states that the height changes (h_x, h_y) of a given perfect matching should be interpreted as the position in the toric diagram of the corresponding GLSM field.

Let us define the following $3 \times N_\sigma$ matrix

$$G_h = \begin{pmatrix} h_x \\ h_y \\ 1 \end{pmatrix} \quad (5.21)$$

The non-trivial piece of G_h is given by (h_x, h_y) . We have included a third row with value 1 for all perfect matchings that plays the role of the trivial coordinate of the toric diagram.

Our goal is to prove that G_h defines the GLSM charge matrix Q through the vanishing linear relations among its columns, and thus can be identified with G in (3.9). I.e. we want to show that

$$Q G_h^T = 0 \quad \Leftrightarrow \quad \begin{array}{l} Q_F G_h^T = 0 \\ \text{and } Q_D G_h^T = 0 \end{array} \quad (5.22)$$

For the third row of G_h , (5.22) means that the trace over perfect matchings of any given GLSM $U(1)$ charge vanishes. It is straightforward to see that this condition is always satisfied. Thus, from now on we concentrate on the (h_x, h_y) piece of G_h .

Let us first show that $Q_F G_h^T = 0$. From (5.23), we have

$$T Q_F^T = 0 \quad (5.23)$$

Hence, it is sufficient to prove that h_x and h_y are given by linear combinations of the rows of T . It is straightforward not only to show that this is the case but also to identify the precise form of these linear combinations. The key ideas are the interpretation of height changes as horizontal and vertical net flows as discussed in Section 2.2 and that KT is computed as the “overlap” of perfect matchings and edges (5.16). With this in mind, we can express the height changes as

$$h_x(p_\alpha) = \sum_j \left(\sum_{e_i \in E_x} \text{sign}^x(e_i) K_{ij} \right) T_{j\alpha} \quad (5.24)$$

$$h_y(p_\alpha) = \sum_j \left(\sum_{e_i \in E_y} \text{sign}^y(e_i) K_{ij} \right) T_{j\alpha} \quad (5.25)$$

where E_x and E_y denote the set of edges crossing the horizontal and vertical boundaries of the unit cell (i.e. the flux lines \mathcal{C}_x and \mathcal{C}_y), and $\text{sign}^x(e_i)$ and $\text{sign}^y(e_i)$ indicate the direction of the crossing. For illustration, let us consider our dP_2 example, for which

$$\begin{aligned} E_x &= \{X_{52}, X_{53}, Y_{23}\} & \text{sign}^x(e_i) &= \{-1, 1, -1\} \\ E_y &= \{X_{23}, Y_{23}\} & \text{sign}^y(e_i) &= \{1, -1\} \end{aligned} \quad (5.26)$$

Figure 9 shows E_x and E_y in the tiling.

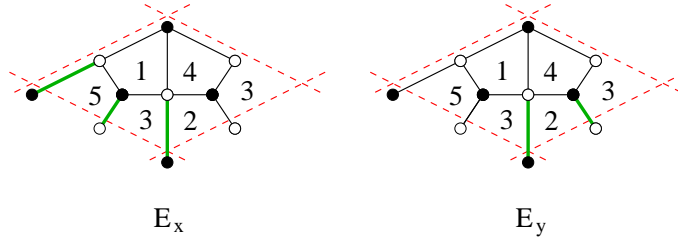


Figure 9: Sets of edges E_x and E_y that enter the computation of (h_x, h_y) .

Using (5.23), the fact that (h_x, h_y) is given by the linear combinations constructed in (5.24) and (5.25) implies that

$$Q_F G_h^T = 0 \quad (5.27)$$

as we want. The missing part of the proof is to show that $Q_D G_h^T = 0$. This can be done as follows

$$\begin{aligned}
(Q_D G_h^T)_{lx} &= \sum_{e_i \in E_x} \text{sign}^x(e_i) (V U T^T K^T)_{li} = \sum_{e_i \in E_x} \text{sign}^x(e_i) (V K^T)_{li} \\
&= \sum_{e_i \in E_x} \text{sign}^x(e_i) \Delta_{li} = 0
\end{aligned} \tag{5.28}$$

In the first equality we have used (5.24) and (3.7). In the second one, we used (3.6). In the third one, we used (3.5). The last step uses the following reasoning. Every face l of a tiling ($l = 1, \dots, F$) is crossed by \mathcal{C}_x over an even number of edges ⁷. Typically, as in the dP_2 example we are considering in the paper, this intersection number is 0 or 2, but larger values are also possible. Every edge intersected by \mathcal{C}_x corresponds to a field X_i in E_x that transforms either in the fundamental ($\Delta_{li} = 1$) or antifundamental ($\Delta_{li} = -1$) representation of the $SU(N)$ gauge group associated with face l ⁸. Let us consider two edges in e_i and e_j in E_x that are consecutive as we move around face l . Then, $\Delta_{li}/\Delta_{lj} = 1$ or -1 provided e_i and e_j are separated by an odd or even number of edges, respectively. Conversely, $\text{sign}^x(e_i)/\text{sign}^x(e_j) = 1$ or -1 if they are separated by an even or odd number of edges. Hence, we have that $\text{sign}^x(e_i)\Delta_{li}/\text{sign}^x(e_j)\Delta_{lj} = -1$, and thus $\sum_{e_i \in E_x} \text{sign}^x(e_i)\Delta_{li} = 0$.

With identical reasoning, it follows that

$$(Q_D G_h^T)_{ly} = \sum_{e_i \in E_y} \text{sign}^y(e_i)\Delta_{li} = 0 \tag{5.29}$$

From (5.28) and (5.29), we conclude that

$$Q_D G_h^T = 0 \tag{5.30}$$

Hence, we have $Q G_h^T = 0$ and we can identify

$$G_h \equiv G \tag{5.31}$$

We have shown that the slopes of the perfect matchings are the positions of the corresponding GLSM fields in the toric diagram, completing our proof of the Mathematical Dimer Conjecture.

Before closing this section we notice an interesting result that was possible due to the use of dimers. Equations (5.24) and (5.25) give the positions of GLSM fields in the toric diagram directly as linear combinations of rows of KT . Nothing like these expressions was clear from the Forward Algorithm and shows, once again, how dimers manage to pick the natural variables for computing the moduli space.

⁷Actually, a face of the tiling may be crossed by \mathcal{C}_x over an odd number of edges. This happens when there are chiral multiplets transforming in the adjoint representation of the corresponding gauge group. Adjoint fields are represented in the tiling by edges such that the faces at both of its sides are identified (arrows beginning and ending at the same node in the dual quiver). For a field X_i in the adjoint representation of the l^{th} gauge group $\Delta_{li} = 0$ and thus the derivation of (5.28) still holds. The reader should keep in mind this subtlety.

⁸As we explained, it is straightforward to incorporate fields in the adjoint representation to the proof.

6. Conclusions

In this paper we have proved the Mathematical Dimer Conjecture. That is, we have explicitly shown that there is a one-to-one mapping between the GLSM fields that realize the moduli space of a toric quiver and perfect matchings in the brane tiling dual to the periodic quiver. We have also demonstrated that the position of each GLSM field in the toric diagram is given by the slope of the corresponding perfect matching.

We have witnessed how dimers often provide an intuitive interpretation of otherwise obscure steps in the computation of the moduli space. An example of this type is that F-term equations can be easily solved using gauge transformations of weights as shown in Section 5.1. This leads to the magnetic flux variables and \mathcal{V} as natural intermediate variables of the Forward Algorithm.

There are several interesting directions that deserve further investigation. A partial list of them is:

- Our discussion has been limited to toric phases of the gauge theories (i.e. phases in which all the gauge groups have the same rank). Non-toric phases are obtained by performing a Seiberg duality transformation on a node for which the number of flavors is larger than twice the number of colors. It would be interesting to investigate whether some generalization of the brane tiling methods is applicable to these phases.
- Conformal invariance can be broken by incorporating fractional branes (D5-branes wrapped over vanishing 2-cycles in the singular geometry). They modify the ranks of gauge groups in the quiver in a way that can be visualized in the brane tiling as a "chessboard" configuration [51]. The resulting RG flows take the form of duality cascades. It would be worth studying whether such RG flows are captured by some modification of the tiling.
- Recently, there has been a renewed interest in marginal deformations of gauge theories [52] and the construction of their supergravity duals [53]. Given the simplicity with which superpotentials are encoded by brane tilings, it is natural to ask whether and how it is possible to study this problem within this framework.
- It is interesting to explore whether brane dimer methods can be extended to $D(9 - 2p)$ -branes probing p -complex dimensional toric singularities. It is natural to conjecture that the corresponding tilings will be $(p - 1)$ -dimensional and live on a $(p - 1)$ -dimensional torus. The concepts of height function, slopes and characteristic polynomial should be appropriately generalized to $(p - 1)$ dimensions. In analogy to what happens in four dimensions, if these constructions exist in other dimensions, they might be useful for finding possible field theory dualities.
- Another direction is to investigate what is the geometric and gauge theory meaning of brane tilings on the Klein Bottle, such as the one presented in Section 2.1.

Acknowledgements: We gratefully acknowledge the invaluable discussions we have had with A. Hanany, J. Heckman, C. Herzog, A. King and C. Vafa. The work of S. F. is supported by the National Science Foundation Grant No. PHY-0243680. D. V. is supported in part by the CTP and the LNS of MIT and the U.S. Department of Energy under cooperative agreement #DE-FC02-94ER40818.

7. Appendix

Perfect matchings for dP_2

Figure 10 presents the ten perfect matchings for Model II of dP_2 and their slopes.

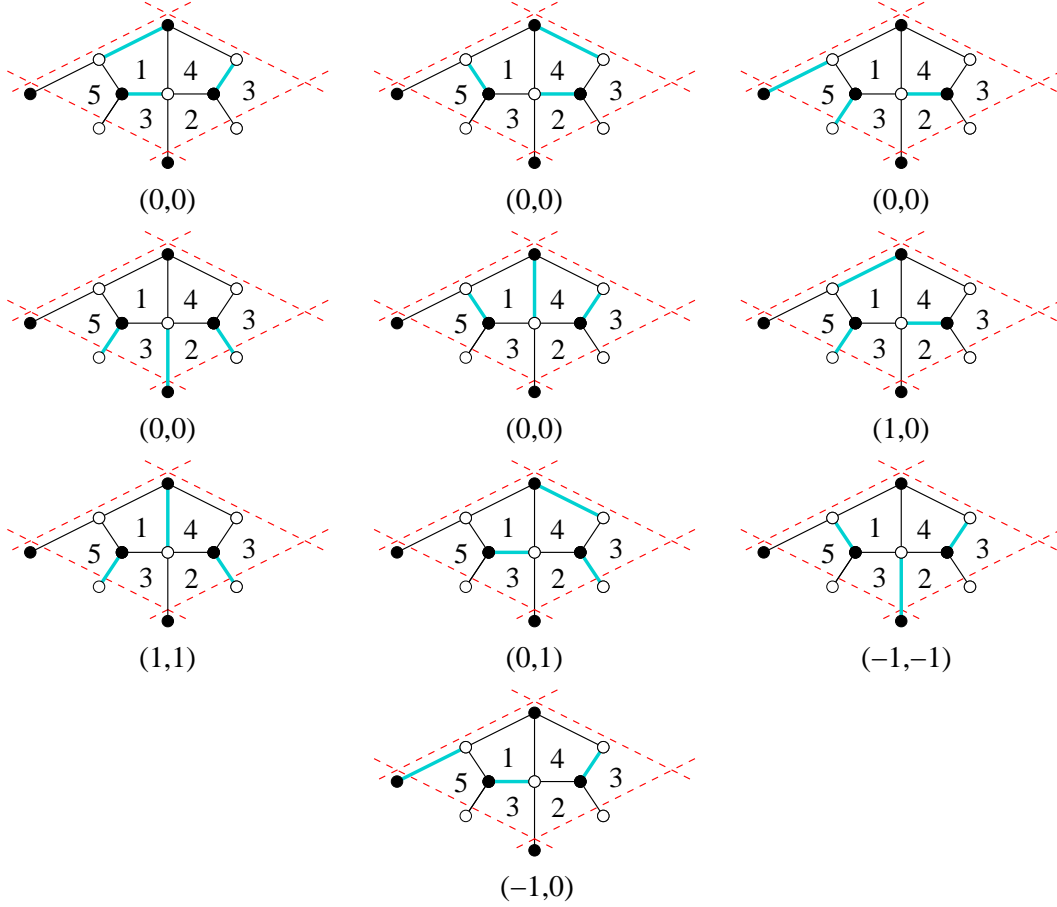


Figure 10: Perfect matchings and their slopes for Model II of dP_2 .

References

- [1] J. M. Maldacena, *The large n limit of superconformal field theories and supergravity*, *Adv. Theor. Math. Phys.* **2** (1998) 231–252, [[hep-th/9711200](#)].
- [2] S. S. Gubser, I. R. Klebanov, and A. M. Polyakov, *Gauge theory correlators from non-critical string theory*, *Phys. Lett.* **B428** (1998) 105–114, [[hep-th/9802109](#)].
- [3] E. Witten, *Anti-de sitter space and holography*, *Adv. Theor. Math. Phys.* **2** (1998) 253–291, [[hep-th/9802150](#)].
- [4] O. Aharony, S. S. Gubser, J. M. Maldacena, H. Ooguri, and Y. Oz, *Large n field theories, string theory and gravity*, *Phys. Rept.* **323** (2000) 183–386, [[hep-th/9905111](#)].
- [5] M. R. Douglas and G. W. Moore, *D-branes, quivers, and ale instantons*, [hep-th/9603167](#).
- [6] M. R. Douglas, B. R. Greene, and D. R. Morrison, *Orbifold resolution by d-branes*, *Nucl. Phys.* **B506** (1997) 84–106, [[hep-th/9704151](#)].
- [7] K. Intriligator and B. Wecht, *The exact superconformal r-symmetry maximizes a*, *Nucl. Phys.* **B667** (2003) 183–200, [[hep-th/0304128](#)].
- [8] J. P. Gauntlett, D. Martelli, J. Sparks, and D. Waldram, *Sasaki-einstein metrics on $s(2) \times s(3)$* , [hep-th/0403002](#).
- [9] J. P. Gauntlett, D. Martelli, J. F. Sparks, and D. Waldram, *A new infinite class of sasaki-einstein manifolds*, [hep-th/0403038](#).
- [10] D. Martelli and J. Sparks, *Toric geometry, sasaki-einstein manifolds and a new infinite class of ads/cft duals*, [hep-th/0411238](#).
- [11] S. Benvenuti, S. Franco, A. Hanany, D. Martelli, and J. Sparks, *An infinite family of superconformal quiver gauge theories with Sasaki-Einstein duals*, [hep-th/0411264](#).
- [12] M. Cvetič, H. Lu, D. N. Page, and C. N. Pope, *New einstein-sasaki spaces in five and higher dimensions*, [hep-th/0504225](#).
- [13] D. Martelli and J. Sparks, *Toric sasaki-einstein metrics on $s^{**}2 \times s^{**}3$* , *Phys. Lett.* **B621** (2005) 208–212, [[hep-th/0505027](#)].
- [14] M. Cvetič, H. Lu, D. N. Page, and C. N. Pope, *New einstein-sasaki and einstein spaces from kerr-de sitter*, [hep-th/0505223](#).
- [15] S. Franco, A. Hanany, D. Martelli, J. Sparks, D. Vegh, and B. Wecht, *Gauge theories from toric geometry and brane tilings*, [hep-th/0505211](#).
- [16] S. Benvenuti and M. Kruczenski, *From sasaki-einstein spaces to quivers via bps geodesics: $Lpqr$* , [hep-th/0505206](#).
- [17] A. Butti, D. Forcella, and A. Zaffaroni, *The dual superconformal theory for $lpqr$ manifolds*, [hep-th/0505220](#).
- [18] D. Martelli, J. Sparks, and S. T. Yau, *The geometric dual of a-maximisation for toric Sasaki- Einstein manifolds*, [hep-th/0503183](#).

- [19] A. Butti and A. Zaffaroni, *R-charges from toric diagrams and the equivalence of a -maximization and z -minimization*, *JHEP* **11** (2005) 019, [[hep-th/0506232](#)].
- [20] Y. Tachikawa, *Five-dimensional supergravity dual of a -maximization*, [hep-th/0507057](#).
- [21] E. Barnes, E. Gorbatov, K. Intriligator, and J. Wright, *Current correlators and ads/cft geometry*, [hep-th/0507146](#).
- [22] D. R. Morrison and M. R. Plesser, *Non-spherical horizons. i*, *Adv. Theor. Math. Phys.* **3** (1999) 1–81, [[hep-th/9810201](#)].
- [23] C. Beasley, B. R. Greene, C. I. Lazaroiu, and M. R. Plesser, *D3-branes on partial resolutions of abelian quotient singularities of calabi-yau threefolds*, *Nucl. Phys.* **B566** (2000) 599–640, [[hep-th/9907186](#)].
- [24] B. Feng, A. Hanany, and Y.-H. He, *D-brane gauge theories from toric singularities and toric duality*, *Nucl. Phys.* **B595** (2001) 165–200, [[hep-th/0003085](#)].
- [25] F. Cachazo, B. Fiol, K. A. Intriligator, S. Katz, and C. Vafa, *A geometric unification of dualities*, *Nucl. Phys.* **B628** (2002) 3–78, [[hep-th/0110028](#)].
- [26] M. Wijnholt, *Large volume perspective on branes at singularities*, *Adv. Theor. Math. Phys.* **7** (2004) 1117–1153, [[hep-th/0212021](#)].
- [27] C. P. Herzog and J. Walcher, *Dibaryons from exceptional collections*, *JHEP* **09** (2003) 060, [[hep-th/0306298](#)].
- [28] C. P. Herzog, *Exceptional collections and del pezzo gauge theories*, *JHEP* **04** (2004) 069, [[hep-th/0310262](#)].
- [29] P. S. Aspinwall and S. Katz, *Computation of superpotentials for d-branes*, [hep-th/0412209](#).
- [30] P. S. Aspinwall and L. M. Fidkowski, *Superpotentials for quiver gauge theories*, [hep-th/0506041](#).
- [31] C. P. Herzog, *Seiberg duality is an exceptional mutation*, *JHEP* **08** (2004) 064, [[hep-th/0405118](#)].
- [32] C. P. Herzog and R. L. Karp, *Exceptional collections and d-branes probing toric singularities*, [hep-th/0507175](#).
- [33] A. Hanany and K. D. Kennaway, *Dimer models and toric diagrams*, [hep-th/0503149](#).
- [34] S. Franco, A. Hanany, K. D. Kennaway, D. Vegh, and B. Wecht, *Brane dimers and quiver gauge theories*, [hep-th/0504110](#).
- [35] A. Hanany and D. Vegh, *Quivers, tilings, branes and rhombi*, [hep-th/0511063](#).
- [36] B. Feng, Y.-H. He, K. D. Kennaway, and C. Vafa, *Dimer models from mirror symmetry and quivering amoebae*, [hep-th/0511287](#).
- [37] A. Butti and A. Zaffaroni, *From toric geometry to quiver gauge theory: The equivalence of a -maximization and z -minimization*, [hep-th/0512240](#).
- [38] N. Seiberg, *Electric - magnetic duality in supersymmetric nonabelian gauge theories*, *Nucl. Phys.* **B435** (1995) 129–146, [[hep-th/9411149](#)].

- [39] C. E. Beasley and M. R. Plesser, *Toric duality is Seiberg duality*, *JHEP* **12** (2001) 001, [[hep-th/0109053](#)].
- [40] B. Feng, A. Hanany, Y.-H. He, and A. M. Uranga, *Toric duality as Seiberg duality and brane diamonds*, *JHEP* **12** (2001) 035, [[hep-th/0109063](#)].
- [41] S. Franco, A. Hanany, Y.-H. He, and P. Kazakopoulos, *Duality walls, duality trees and fractional branes*, [hep-th/0306092](#).
- [42] B. Feng, S. Franco, A. Hanany, and Y.-H. He, *Symmetries of toric duality*, *JHEP* **12** (2002) 076, [[hep-th/0205144](#)].
- [43] S. Benvenuti and M. Kruczenski, *Semiclassical strings in sasaki-einstein manifolds and long operators in $n = 1$ gauge theories*, [hep-th/0505046](#).
- [44] A. Hanany and A. Zaffaroni, *On the realization of chiral four-dimensional gauge theories using branes*, *JHEP* **05** (1998) 001, [[hep-th/9801134](#)].
- [45] A. Hanany and A. M. Uranga, *Brane boxes and branes on singularities*, *JHEP* **05** (1998) 013, [[hep-th/9805139](#)].
- [46] M. Aganagic, A. Karch, D. Lust, and A. Miemiec, *Mirror symmetries for brane configurations and branes at singularities*, *Nucl. Phys.* **B569** (2000) 277–302, [[hep-th/9903093](#)].
- [47] J. A. Bondy and U. S. R. Murty, *Graph Theory with Applications*. North-Holland, 1976.
- [48] R. Kenyon, *An introduction to the dimer model*, [math.CO/0310326](#).
- [49] R. Kenyon, A. Okounkov, and S. Sheffield, *Dimers and amoebae*, [math-ph/0311005](#).
- [50] J. Edmonds, *Maximum matching and a polyhedron with $(0,1)$ -vertices*, *J. Res. Nat. Bur. Standards* **B69** (1965) 125–130.
- [51] S. Franco, A. Hanany, F. Saad, and A. M. Uranga, *Fractional branes and dynamical supersymmetry breaking*, [hep-th/0505040](#).
- [52] R. G. Leigh and M. J. Strassler, *Exactly marginal operators and duality in four-dimensional $n=1$ supersymmetric gauge theory*, *Nucl. Phys.* **B447** (1995) 95–136, [[hep-th/9503121](#)].
- [53] O. Lunin and J. Maldacena, *Deforming field theories with $u(1) \times u(1)$ global symmetry and their gravity duals*, *JHEP* **05** (2005) 033, [[hep-th/0502086](#)].